Available online at www.sciencedirect.com

SCIENCE DIRECT®

Earth and Planetary Science Letters 233 (2005) 121–135

EPSL

www.elsevier.com/locate/epsl

Heterogeneity and time dependence in 3D spherical mantle convection models with continental drift

Benjamin R. Phillips*, Hans-Peter Bunge[1]

Department of Geosciences, Princeton University, Princeton, NJ 08544, USA

Received 24 June 2004; received in revised form 17 January 2005; accepted 23 January 2005

Editor: V. Courtillot

Abstract

Feedback between continents and large-scale mantle flow through thermal blanketing has long been surmised as a mechanism for continental drift and Wilson cycles. Paleomagnetism provides evidence for extensive continental displacements (~ 10,000 km) on time scales of 100–200 million years, comparable to an intrinsic overturn in whole mantle convection. Here we model continental motions in vigorous 3D spherical convection models, focusing on the effects of continent size, mantle heating mode, and a strong increase in lower mantle viscosity. Continents covering 30%, 10%, and 3% of Earth's surface (representative of the former supercontinent Pangea, present-day Asia, and Antarctica, respectively) are introduced into simple end member mantle convection models characterized by pure core or internal heating, and uniform or layered mantle viscosity. Supercontinents promote temperature anomalies on the largest scales (spherical harmonic degrees 1 and 2), primarily through the organization of the long-wavelength convective planform inherent in models with a high-viscosity lower mantle. Bottom heating can promote long-wavelength heterogeneity by clustering plumes beneath the continent. However, in isoviscous models small-scale structure persists away from the continent regardless of the heating mode. Supercontinents respond to long-wavelength heterogeneity by following great circle paths with variations in velocity on time scales of 1 billion years. Smaller continents are unable to promote long-wavelength structure, and the resulting motions are governed by bursts in velocity on time scales of the order of 100 million years. Continental velocities are roughly a factor of ~ 3 smaller than those in oceanic regions, an observation that may help explain the observed difference in the speed of predominantly continental or oceanic plates.

Keywords: mantle convection; continental drift; supercontinent

1. Introduction

In an influential 1982 paper, Anderson [1] noted a correlation between the Atlantic–African geoid high and the Jurassic location of the supercontinent

* Corresponding author.
E-mail address: benp@princeton.edu (B.R. Phillips).
[1] Present address: Institut für Geophysik, Universität München, Theresienstrasse 41, 80333 München, DE.

0012-821X/$ - see front matter © 2005 Elsevier B.V. All rights reserved.
doi:10.1016/j.epsl.2005.01.041

Pangea. Through this observation he suggested that continents could promote the growth of broad thermal anomalies in the Earth, both by shielding the underlying mantle from subduction and by providing a thermal blanket, leading to an increase in mantle temperatures beneath continents by perhaps 50–100 K over time periods of order 100 million years (Myr).

Anderson's proposition sparked a series of geodynamic simulations to test the continental insulation hypothesis. Gumis [2] included the effect of continents in two dimensional (2D) Cartesian models heated purely from below. He concluded that continents insulate the mantle and ultimately lead to subcontinental heating through the clustering of plumes. In a series of laboratory convection experiments also heated only from below, Guillou and Jaupart [3] observed the emplacement of upwellings and the development of large-scale flow patterns, in response to a conductive lid at the surface. The reduction in heat flow through continents may also be modeled more directly by following the Biot number [4,5]. Zhong and Gumis [6] added modest amounts of radiogenic internal heating to their numerical models. They found that periods of rapid continental motion occurred in response to the development of large-scale mantle heterogeneity, implying a dynamic feedback between continents and the pattern of mantle convection. In a series of papers, Lowman and Jarvis [7,8] and Lowman and Gable [9] investigated the effects of mixed internal and bottom heating, verifying that continental insulation promotes long-wavelength structure in models with strong heating from the core. However, this effect is less pronounced in three-dimensional (3D) convection models, owing to the proper representation of plumes as narrow cylinders instead of as 2D sheets. Furthermore, for predominantly internally heated flow as expected in the mantle, Lowman and Gable showed that subcontinental heating results from an absence of subduction rather than from the insulation of active upwellings. Yoshida et al. [10] also suggested pronounced subcontinental heating based on 3D spherical calculations with a stationary high-viscosity lid and ~ 70–80% internal heating.

The ratio of internal, radioactive heat generation in the mantle relative to the amount of heat entering from the core has recently received renewed attention. Internal heating due to radioactive decay is the primary source in the mantle thermal budget [11]. Still, the amount of core heating is poorly known. Classic arguments based on the dynamic topography over mantle hotspots suggest a modest core contribution to the mantle energy budget, on the order of 5–10% [12,13]. However, recent geodynamic studies favor significantly higher values to overcome problems of insufficient internal heat sources [14], and to satisfy constraints on power requirements of the geodynamo and the thermal history of the core [15–17]. Significant heat flux from the core into the mantle is also suggested by the non-adiabatic mantle geotherm arising from internal mantle heating [18]. Consequently, current estimates of core heating based on hotspot topography could be increased by as much as a factor of 3 [19].

The dominance of long-wavelength heterogeneity in the Earth's mantle is now widely agreed upon. For example, Su and Dziewonski [20] noted a peak in seismic heterogeneity in the lower mantle near spherical harmonic degree 2, corresponding to spatial scales of 20,000 km. Recent high-resolution seismic models confirm the preponderance of long-wavelength mantle flow [21–23]. These seismic images support the notion of a mantle containing plumes clustered beneath Africa and the Pacific in a broad zone of mantle upwelling, separated by a ring of cold, downwelling slabs that correlate with the history of Mesozoic and Cenozoic subduction [24,25]. Large-scale mantle structure is also evidenced by the geoid, Earth's equipotential surface. The geoid is elevated over the African and Pacific hemispheres, as noted by Anderson [1], and corresponds closely to the distribution of mantle hotspots [26].

In vigorous 3D mantle convection models, a long-wavelength planform is promoted primarily by a strong increase in viscosity with depth [27,28]. To a lesser degree convective length scales are influenced by the ratio of internal to bottom heating [29,30], with bottom heating promoting longer wavelength heterogeneity. When combined with the effects of plates at the surface, mantle flow with a depth-dependent viscosity is organized into the longest spatial scales, corresponding to spherical harmonic degree 2 [31,32]. Evidence for a depth-wise increase in viscosity derives from models of the geoid [33,34] and studies of post glacial rebound [35], both of which suggest an increase in viscosity by a factor of 10–100 from the

upper to the lower mantle. Plate-like behavior, and hence long-wavelength convection, may also be accomplished by introducing complex rheologies for the model fluid (e.g. [36–38]).

Paleomagnetic studies of the past decade have produced detailed apparent polar wander paths for many continents [39]. These studies provide important constraints on the temporal character of mantle flow for time periods of several mantle overturns and establish continental motions that are both extensive in range and highly time dependent. Paleozoic [40] and Mesozoic [41] continents traversed sizable portions of the globe (~ 10,000 km) and exhibited bursts in velocity, such as for India, comparable to modern oceanic plate velocities. Evidence also suggests episodes of true polar wander [42], perhaps related to inertial interchanges, that could be expressed by extremely rapid continental velocities [43,44]. By comparison, continents today move relatively slowly [45], and on average the root mean square (RMS) velocities of predominantly oceanic plates exceed continental velocities by a factor of 3 to 4 [46].

In this paper we study the continental drift problem using high-resolution 3D spherical models of mantle convection with a freely moveable continental cap. We seek to elucidate the effect of continents on the development of mantle heterogeneity in relatively simple end-member mantle convection models, devoid of unnecessary complexities. Because of the strong influence of a depth-wise increase in viscosity on the convective planform, we study models with uniform and depth-dependent viscosity. Owing to the potential importance of bottom heating, we also investigate the influence of heating mode, with models heated either purely from below or purely from within the mantle. To probe the sensitivity of these results to variations in continental size, we include continents covering 30%, 10%, and 3% of Earth's surface, representative of the former supercontinent Pangea, present-day Asia, and Antarctica, respectively.

We begin by first presenting the equations used to model mantle convection, followed by a brief description of our numerical solution methods. After a description of our model parameters, we describe the method used to prescribe the continent and to couple its motion to the underlying mantle flow. Next, we present temperature fields for four reference mantle convection models without a continent, characterized by pure bottom or internal heating, and uniform or layered mantle viscosity. We then compare these reference calculations to identical cases that include a supercontinent. Using spectral heterogeneity maps (SHMs), we quantify the effect of the supercontinent on the spatial scales of flow in our models. The SHMs are followed by time series of continental latitude, RMS surface velocities, and mid-mantle temperatures in regions both beneath and away from the supercontinent. Finally, we contrast these results with cases involving smaller continents.

2. Modeling approach

2.1. Governing equations

Mantle convection is described quantitatively by equations expressing the conservation of mass, momentum, and energy (e.g. [47]) for a highly viscous fluid,

$$\nabla \cdot \boldsymbol{u} = 0 \tag{1}$$

$$-\nabla p + \mu \nabla^2 \boldsymbol{u} + \alpha \rho \Delta T \boldsymbol{g} = 0 \tag{2}$$

$$\frac{\partial T}{\partial t} + \boldsymbol{u} \cdot \nabla T = \kappa \nabla^2 T + \frac{Q}{\rho^2 C_\mathrm{p}} \tag{3}$$

Here $\boldsymbol{u}$ is the velocity of the fluid, p is the pressure, μ is the viscosity, α is the thermal expansivity, ρ is the density, T is the temperature, $\boldsymbol{g}$ is the gravitational acceleration, Q is the rate of internal heating per unit mass, C_p is the specific heat at constant pressure, and $\kappa = K/\rho C_\mathrm{p}$ is the thermal diffusivity (K is the thermal conductivity). Assuming that the mantle is incompressible, Eq. (1) simply expresses a volume conservation. The momentum Eq. (2) poses a balance primarily between viscous forces $\mu \nabla^2 \boldsymbol{u}$ and the thermal buoyancy force $\alpha \rho \Delta T \boldsymbol{g}$. This is a simplification as inertial forces and temporal variations in $\boldsymbol{u}$ are ignored. Both are sufficiently small for the extremely viscous flow of the mantle, and the momentum balance is therefore instantaneous. Time dependence is introduced into the system through the energy Eq. (3), where temporal variations in temperature $\partial T/\partial t$ are balanced by heat advection $\boldsymbol{u} \cdot \nabla T$ and diffusion $\kappa \nabla^2 T$.

Appropriate boundary conditions for the mantle are free-slip (no shear stress), zero radial velocity (no in- or out-flow), and constant temperature T_B=3000 K and T_O=300 K on the inner {B} and outer surfaces {O}. In our cases including pure internal heating, the bottom boundary condition changes from isothermal to insulating, while the outer surface remains isothermal. We then have

$$T(x) = T_O(x) \qquad x \in \{O\} \tag{4}$$

$$T(x) = T_B(x) \qquad x \in \{B\} \text{ or} \tag{5}$$

$$\nabla T(x) \cdot \hat{\boldsymbol{n}} = 0 \qquad x \in \{B\} \tag{6}$$

$$\nabla \boldsymbol{u}(x) \cdot \hat{\boldsymbol{n}} = 0 \qquad x \in \{B,\ O\} \tag{7}$$

$$\boldsymbol{u}(x) \cdot \hat{\boldsymbol{n}} = 0 \qquad x \in \{B,\ O\} \tag{8}$$

Eqs. (1)–(8) are solved numerically in a spherical shell with an outer radius corresponding to the Earth's surface and an inner radius corresponding to the core-mantle boundary (CMB). We use a modified version of the 3D spherical finite element mantle convection code Terra [48,49]. The code, which has been benchmarked to 1% accuracy [32], employs an efficient multigrid solver for computing a solution to the momentum Eq. (2). The energy Eq. (3) is solved using an Eulerian advection scheme. Models presented here are incompressible and implemented in a mesh containing more than 10 million finite elements, yielding a grid spacing of ~ 50 km.

For all models we implement a uniform convective vigor. This is gauged by the thermal Rayleigh number, defined for bottom heating as

$$Ra_b = \frac{\alpha g \rho \Delta T d^3}{\mu \kappa} \tag{9}$$

where ΔT is the temperature difference across the mantle, d is the mantle depth, and all other quantities are as defined in Eqs. (2) and (3). We model purely bottom-heated convection at $Ra_b = 10^6$. For internally heated mantle convection models, the temperature difference ΔT in (9) is replaced by $Qd^2\rho/K$ [50]. The internally heated Rayleigh number is then

$$Ra_i = \frac{\alpha g \rho^2 Q d^5}{\mu \kappa K} \tag{10}$$

Equivalent convective vigor (determined by matching the surface heat flux) yields $Ra_i = 10^7$ for internally heated models. This is likely one to two orders of magnitude smaller than for the Earth [51]. Computational resources limit the resolution of our grid, so such a reduction in the Rayleigh number is necessary to resolve the thermal boundary layers of ~250 km thickness in our models. To reduce the Rayleigh number, we increase the viscosity μ over the value inferred for Earth's mantle (10^{21} Pa s for the upper mantle [35,52]).

2.2. End member mantle convection models

We focus on four end member cases characterized by pure bottom or internal heating, and uniform or layered mantle viscosity. Our first case has a constant viscosity of 1.374×10^{23} Pa s and is heated only from the bottom. The CMB is held at a fixed temperature T_B=3000 K, yielding a surface heat flow of 10 TW. Case 2 is also bottom-heated with the same fixed temperature at the CMB, but includes the addition of a viscosity increase of a factor of 30 from the upper to lower mantle. The upper mantle viscosity of 6.483×10^{21} Pa s increases by a factor of 3 at 540 km depth, to a factor of 10 larger at 587 km, and finally to a lower mantle viscosity of 1.945×10^{23} Pa s below 632 km. We maintain the same surface heat flow (10 TW) in this model by effectively keeping the volume averaged viscosity constant. For case 3, the mantle is again isoviscous at 2.391×10^{23} Pa s, but the CMB is left as an insulating boundary. Heating in this case is accomplished purely from within using a radiogenic heating rate of $Q = 3 \times 10^{-12}$ W/kg. This provides a surface heat flow of 10 TW, as in the two bottom-heated cases. Case 4 is similarly heated only from within, and includes a layered viscosity structure following case 2, beginning with an upper mantle viscosity of 1.128×10^{22} Pa s and transitioning to a lower mantle viscosity of 3.384×10^{23} Pa s. Using the volume averaged viscosity, the volume-averaged Rayleigh numbers for our bottom and internally heated cases are then 10^6 and 10^7, respectively.

As the Rayleigh number in our models is lower than that of the Earth, model velocities are smaller, and model times longer than for the Earth. We observe time averaged RMS surface velocities of 0.3 cm/yr, 0.1 cm/yr, 0.8 cm/yr, and 0.7 cm/yr, respectively for

the four cases described above. For our results, we scale these model velocities and hence the model times to a mean surface velocity of 5 cm/yr, representative of present day RMS plate velocities [46]. We refer to these scaled values throughout the remainder of this paper.

All cases were first run until a quasi-steady convection state was reached. As our models are highly time-dependent, we define the steady state as one in which the total heat flux into and out of the system is balanced.

2.3. Continental formulation

Continents are characterized to first order by the fact that they do not subduct or experience significant internal deformation. Therefore, we approximate continents as buoyant, perfectly rigid caps. Following Davies [53], we fix a surface temperature T_C over the continental region $\{C\}$ equal to the mean mantle temperature at the base of the upper thermal boundary layer (250 km depth). This eliminates the potential for material directly beneath the continental footprint to cool and subduct, while effectively preventing heat loss through the surface. Such behavior is appropriate given that the mean heat flux through the continents is about half that through the oceanic lithosphere [54]. Following the method of Gable et al. [55] we compute continental velocities from a torque balance. Continents are imposed as semi-spherical caps with borders defined by small circles on the surface of the sphere (see Fig. 1). Tractions are computed at each grid point of the continent and integrated over the continental area. A steepest ascent algorithm is used to calculate the Euler rotation vector ω that minimizes the torques exerted on the continent by the underlying flow. Fig. 1 summarizes this process. Thermal and mechanical boundary conditions for the continental surface are then

$$T(x) = T_C(x) \qquad x \in \{C\} \tag{11}$$

$$u(x) = \boldsymbol{\omega} \times \hat{\mathbf{r}}(x) \qquad x \in \{C\} \tag{12}$$

$$u(x) \cdot \hat{\boldsymbol{n}} = 0 \qquad x \in \{C\} \tag{13}$$

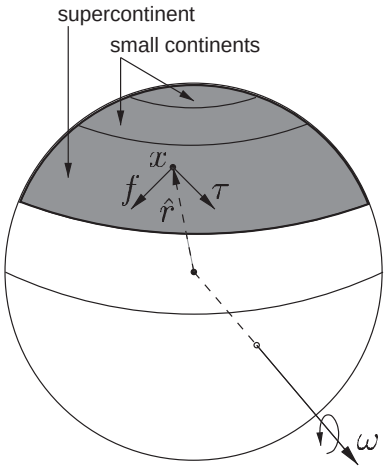

Fig. 1. Schematic view of the 3D spherical domain showing a continental cap in gray. The entire gray region is representative of a supercontinent (e.g. Pangea) covering 30% of the surface. The upper portion shows regions occupied by smaller continents covering only 10% or 3% of the surface (approx. Asia or Antarctica, respectively). The unit vector $\hat{\mathbf{r}}$ points from the center of the sphere to a continental node located at x. This node experiences a viscous force $\boldsymbol{f}$ and torque $\boldsymbol{\tau} = \hat{\mathbf{r}} \times \boldsymbol{f}$ imparted by the flow below. An Euler rotation vector ω is found by minimizing the sum of all such torques over the continent.

Eqs. (11)–(13) are incorporated into the solution strategy defined in Section 2.1.

3. Results

3.1. Temperature fields and convective planform

Fig. 2.1A–4A show snapshots in time of the evolving temperature fields for our four reference mantle convection calculations without continents. Temperatures range from hot (red) to cold (blue), with values as indicated by the color bars. The inner spherical boundary shows the CMB. The outer boundary is set at 90 km depth, revealing flow structures directly beneath the surface.

The bottom-heated, isoviscous reference case 1A exhibits flow dominated by hot plume-like upwellings originating from the CMB, surrounded by downwellings in the form of cylindrical sheets. The uniform, red inner boundary represents the fixed CMB temperature of 3000 K. Increasing the lower mantle viscosity in Fig. 2.2A does not significantly alter these

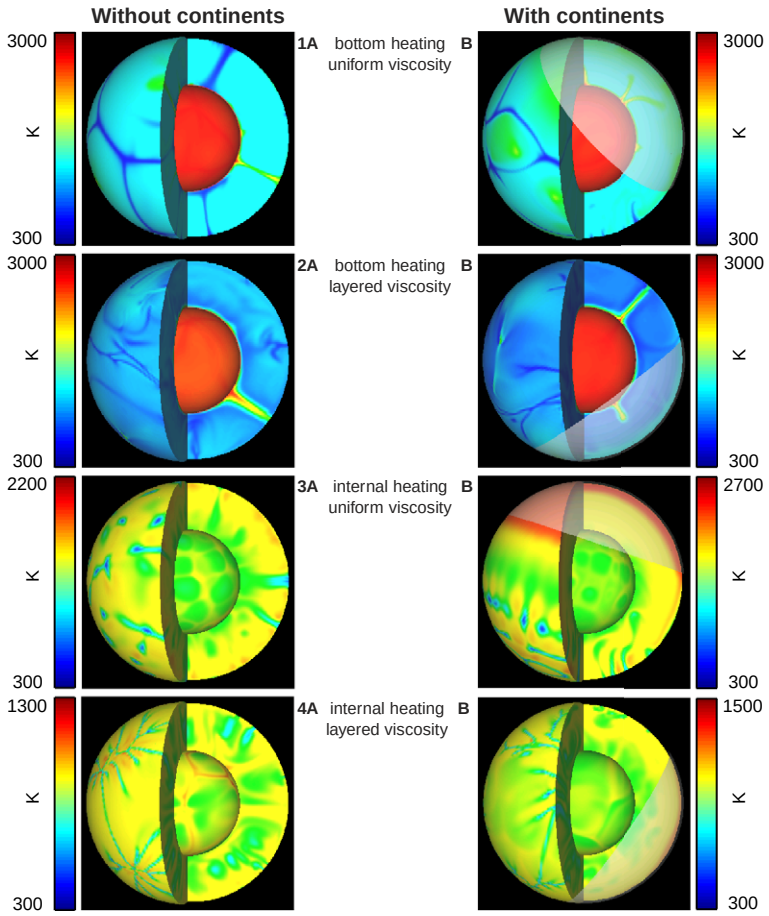

Fig. 2. Temperature field snapshots for eight cases with bottom or internal heating and uniform or layered viscosity (with an increase by 30× from the upper to the lower mantle). Temperatures run from hot (red) to cold (blue), with values given by the color bars. The inner and outer spherical boundaries correspond to the core–mantle boundary (CMB) and 90 km depth, respectively. Left: Cases lA–4A correspond to convection calculations without continents. In 1A and 2A flow is driven by hot plumes rising from the CMB, surrounded by cold, cylindrical downwelling sheets. In 3A plume-like downwellings dominate the flow, while 4A exhibits downwelling sheets. Right: lB–4B show cases with a supercontinent covering 30% of the surface (gray cap). Plumes concentrate beneath the continent in lB, but the continent in 2B has little apparent impact. The sub-continental mantle is hotter in 3B, although small downwelling plumes persist in the opposite hemisphere. In 4B the mantle is again hotter beneath the supercontinent, with downwellings confined to the oceanic hemisphere.

structures, although the spacing between plumes increases. In the internally heated, isoviscous model in Fig. 2.3A there is no longer a hot thermal boundary layer at the CMB due to the lack of core heating. Flow in this case is dominated by downwelling plumes spaced by roughly 2000 km. These downwellings are distinct in the upper half of the mantle and become more diffuse at greater depth. Increasing the lower mantle viscosity has a strong effect on the convective planform of the internally heated case in Fig. 2.4A. The downwellings are no longer plume-like, but form narrow, continuous bands. These characteristics of 3D spherical mantle convection without continents have been described in detail before [29,30,56].

We now turn our attention to the four cases that include the effects of a supercontinent. Fig. 2.1B shows the temperature field for the purely bottom-heated, isoviscous case. The supercontinent covers 30% of the surface and is designated by a transparent gray cap. The calculation is shown at the end of the total integration time of 3000 Myr. Note that we initially centered the continent at the North Pole, and

its present position to the side indicates drift over the course of the model integration. As expected, plumes cluster beneath the continent, which isolates the underlying mantle from cold downwellings. However, additional plumes persist outside of the continental area. These plumes are weaker than plumes in the reference case without a continent (Fig. 2.1A), as indicated by a closer spacing of the downwelling sheets, resulting in shorter overall spatial heterogeneity scales. The continent has little effect on mantle temperature in the bottom-heated, layered viscosity case shown in Fig. 2.2B, although there is an emergent plume rising directly beneath the continent. The isoviscous, internally heated model with a supercontinent is shown in Fig. 2.3B, again after 3000 Myr of integration time. In this case the continent moved rather little from its initial position at the North Pole. Hot mantle impinges directly beneath the insulating continent, and in a zone abutting the continent this material is transported horizontally towards the opposite hemisphere to cool. Away from the continent, in the oceanic hemisphere, flow is dominated by small-scale downwelling plumes as seen earlier in the reference case with no continent (Fig. 2.3A). We turn finally to the internally heated, layered viscosity case in Fig. 2.4B. Here we observe large-scale flow with long linear downwellings, similar to the reference case without a continent (Fig. 2.4A). Owing to the insulating effect of the continent, the network of interconnected downwellings is clustered in the oceanic hemisphere, while relatively warm mantle rises beneath the continent. We note that the continent moved from its initial position at the North Pole to a final position in the Southern Hemisphere.

3.2. Spectral heterogeneity maps

We quantify the heterogeneity character in our models with spectral heterogeneity maps [56]. Fig. 3.1A–4A and Fig. 3.1B–4B show SHMs for the reference and supercontinent cases, respectively. These SHMs were calculated for the snapshots of Fig. 2, but are representative of the spectral character observed throughout the evolution of the models. Each panel shows a contour plot of the spectral amplitude of the temperature field as a function of spherical harmonic degree from 0 to 32, and mantle depth from the base of the lithosphere to the CMB. The panels are normalized individually by their maximum amplitude and stronger heterogeneities are indicated by darker shading.

For the bottom-heated, isoviscous reference case in Fig. 3.1A structure is dominated by spherical harmonic degrees 4–8, due to upwelling plumes. As expected, the amplitudes are greatest near the upper and lower thermal boundary layers. Some weaker mid-mantle heterogeneity near degrees 16 and 24 is due primarily to downwelling sheets. Fig. 3.2A indicates that the addition of a viscosity jump in the lower mantle attenuates small-scale structure, and concentrates the strongest features about spherical harmonic degree 4. The dominance of small-scale structure seen in the planform of the isoviscous, internally heated case in Fig. 2.3A is evident in the SHM of Fig. 3.3A. A large amount of heterogeneity is revealed throughout mantle above spherical harmonic degree 16. Note that the dominant peaks between degrees 20 and 28 correspond directly to the ~ 2000-km-length scale inferred for the spacing of downwellings seen in the temperature field in Fig. 2.3A. At greater depth these features fade in strength and broaden in width, as noted before. Finally, for the internally heated convection model with a high viscosity lower mantle, Fig. 3.4A reveals a substantial shift of spectral heterogeneity towards longer wavelengths between spherical harmonic degrees 4 and 8 in the lower mantle. This shift reflects the long-wavelength planform characteristic of mantle convection with depth-dependent viscosity.

Having examined the SHMs in our reference cases without continents, we next turn our attention to the four cases with supercontinents. For the bottom-heated isoviscous case, we see in Fig. 3.1B that the supercontinent shifts the spectrum towards the longest length scales (~ 10,000 km), with a degree 1–2 feature dominating throughout the mantle. Still, there is some small-scale structure (spherical harmonic degrees 4–16) due to weaker plumes away from the continent, as noted earlier in the temperature fields. By comparison, the difference in spectral heterogeneity between the bottom-heated, layered viscosity case with (Fig. 3.2B) and without (Fig. 3.2A) the continent is minor. This is in agreement with our earlier observation from the

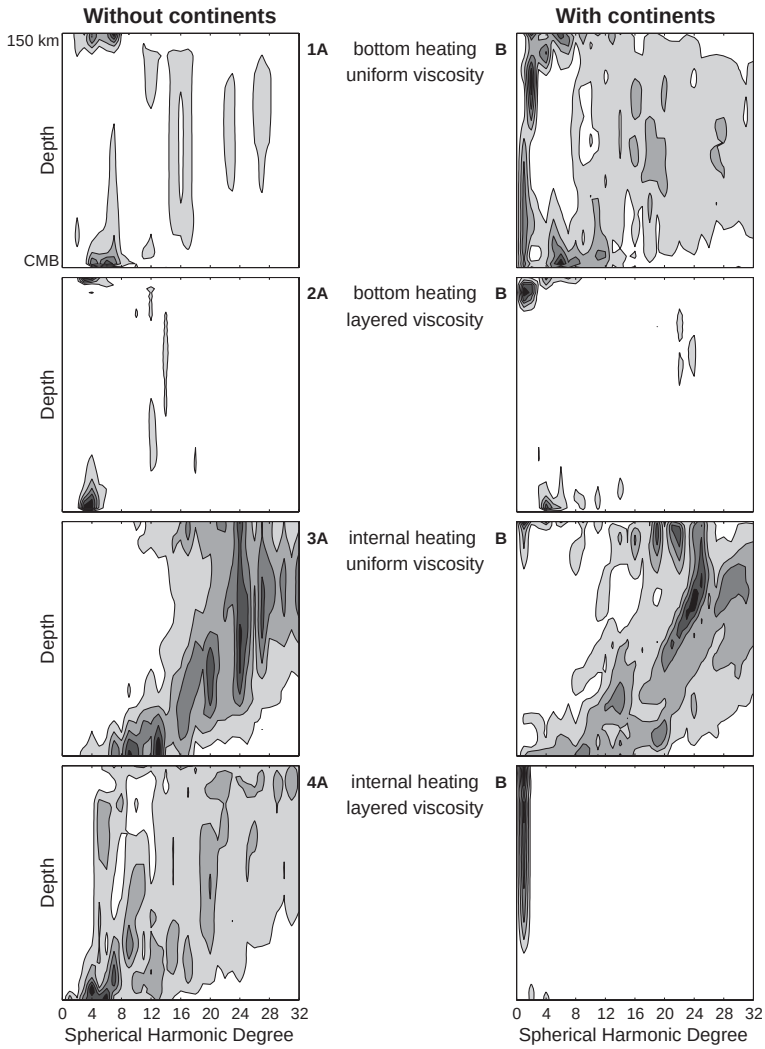

Fig. 3. Spectral heterogeneity maps (SHMs) of temperature for the eight snapshots of Fig. 2. Root mean square (RMS) spectral amplitude is plotted as a function of mantle depth (from the base of the lithosphere to the CMB) and spherical harmonic degree (from 0 to 32). There are five contour intervals and darker shading corresponds to larger amplitude. Each panel is normalized by the maximum amplitude in that panel. Left: Without continents. In 1A amplitudes are greatest near the thermal boundary layers, peaking at degrees 4–8. This shifts to longer wavelengths (degree 3 to 4) in 2A. In 3A we see significant small scale structure between degrees 20 and 28. Case 4A is characterized by degree 4 in the lower mantle. Right: With supercontinents. For 1B small scale structure remains, but with a new degree l–2 feature arising throughout the mantle. In 2B new structure at degree 2 is confined to the upper mantle. 3B is much like 3A, save new degrees l–8 structure near the upper boundary layer. In 4B a strong degree 1 feature dominates.

temperature fields, where we noted that the continent had little overall impact on the convective planform. Similarly, the SHM of the internally heated, isoviscous case with a supercontinent (Fig. 3.3B) is remarkably similar to the reference case with no continent (Fig. 3.3A). While there is some long-wavelength structure in the upper most mantle at spherical harmonic degrees l–8 due to the continent, small-scale structure prevails throughout the rest of the mantle. The supercontinent has the most dramatic impact in the internally heated, layered viscosity case shown in Fig. 3.4B. Here mantle flow is dominated by a prominent degree 1 feature completely absent in the reference case without a continent.

3.3. Time dependence and supercontinents

We examine the temporal behavior of our models with supercontinents in Fig. 4. The top four panels show the latitude of the center of the supercontinent as a function of time. While the continents were always centered initially at 90° latitude, the time series show only the last 3000 Myr for each case. Some drift occurred during additional time prior to 0 Myr as the calculation was allowed to equilibrate. In the bottom-heated, isoviscous case 1 there is relatively little time dependence, as the supercontinent moves uniformly from one pole to the other and back with a period of ~ 1500 Myr. For case 2, with bottom heating and layered viscosity, the supercontinent again exhibits large-scale motions. However, because the continent in this case moves predominantly in equatorial regions, there is now relatively little latitudinal variation. For the internally heated, isoviscous case 3 with predominantly small-scale flow, the continent

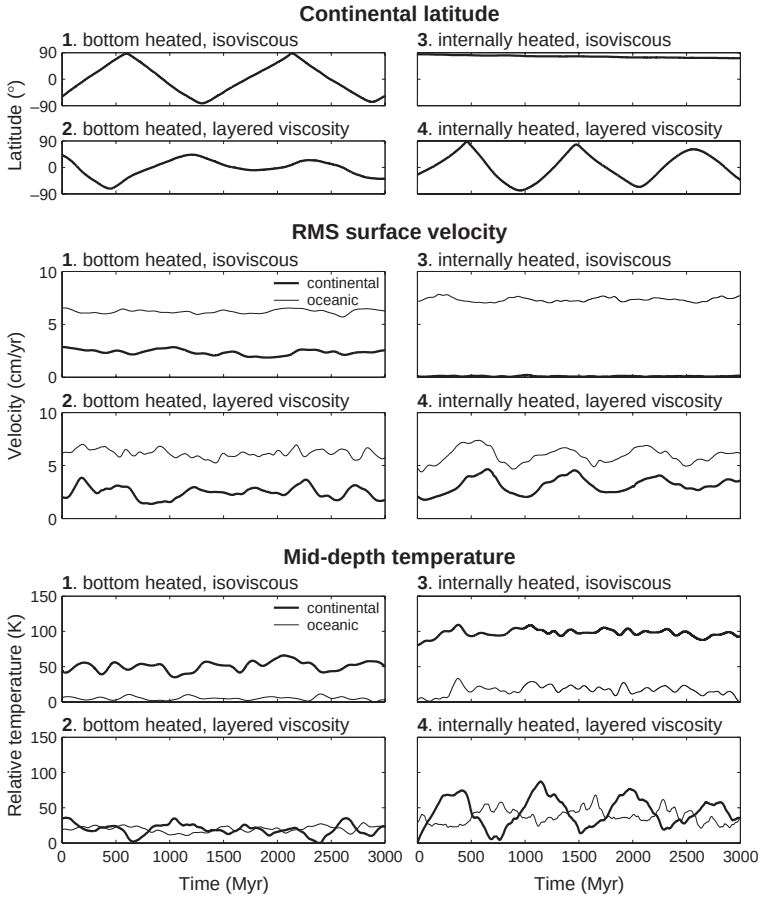

Fig. 4. Time series for 3000 Myr for the four supercontinent cases of Fig. 2. Top: Latitude of the supercontinent center. For case 1 the continent follows a great circle path, moving from one pole to the other and back in 1500 Myr. The path is less regular for case 2. In case 3 the continent moved only 10° over the entire 3000 Myr. In case 4 the motion is again oscillatory, with period of 1000 Myr. Middle: RMS surface velocities for the supercontinent (thick line) and the remainder of the surface, or oceanic regions (thin line). In all cases continental velocities are at least 2–3 × slower than oceanic velocities. Continental velocities are relatively uniform in case 1, but variable from 2 to 4 cm/yr in case 2. In case 3 the continent is stagnant. For case 4 velocity varies periodically from 2 to 5 cm/yr over 800 Myr. Bottom: Mean temperature variations at mid-mantle depth for each case under the supercontinent (thick line) and under the oceans (thin line). For case 1 the sub-continental mantle is 50 K warmer than the surrounding mantle. In case 2 there is no appreciable difference. The mantle is 80 K warmer beneath the continent in case 3. In case 4 sub-continental temperatures vary by ~ 80 K with a period of 800 Myr, mirrored by the above changes in velocity.

is virtually stagnant. This is evident from Fig. 4, where the continent remains near the North Pole for the entire model duration, drifting by only ~ 10° over 3000 Myr (< 1 mm/yr). In contrast, motion for the internally heated, layered viscosity case 4 is again cyclic from pole to pole, with the period for one great circle path lasting ~ 1000 Myr.

In the middle four panels of Fig. 4 we show the RMS velocity of the supercontinent (thick line) and the remainder of the surface, or oceanic regions (thin line). The most striking observation here is the disparity between the RMS velocity in oceanic and continental regions, with continents moving on average a factor of 3 slower than oceanic regions in all four cases. Oceanic RMS surface velocities range between 6 and 8 cm/yr, while supercontinental velocities range from l to 5 cm/yr. We also note that there is generally more time dependence in the RMS velocity of the continent in cases with layered mantle viscosity. In the bottom-heated layered viscosity case 2, for example, we observe continental velocities varying from l to 4 cm/yr, with fluctuations occurring over time periods of 200–300 Myr. In contrast, the continent in the bottom-heated, isoviscous case 1 moves at a relatively steady velocity of 2–3 cm/yr. Continental velocities in the internally heated case 4 vary between 2 and 5 cm/yr with a period of ~ 800 Myr. RMS surface velocities in the oceanic regions vary on the same time scale. As mentioned previously, the continent in the internally heated, isoviscous case 3 is almost stationary, with an average velocity of 0.9 mm/yr.

We gain physical insight into the surface velocity variations by looking at temperature changes in the underlying mantle. The bottom four panels of Fig. 4 show time series of mean temperature variations at mid-mantle depth (1500 km), both for subcontinental (thick line) and suboceanic regions (thin line). In the two isoviscous cases there are persistent lateral temperature variations between subcontinental and suboceanic regions due to the clustering of plumes and broad mantle upwellings beneath the continent. As a result temperatures beneath the continent exceed suboceanic mantle temperatures by 50–80 K. Cases with depth-dependent viscosity do not exhibit such regular variations in mantle temperature, due to the long-wavelength convective planform. For the bottom-heated, layered viscosity case the difference in temperature between the subcontinental and suboceanic mantle averages less than 10 K. In the internally heated, layered viscosity case subcontinental temperatures vary by about 80 K on a time scale of ~ 800 Myr, comparable to the periodicity noted for the RMS surface velocities.

3.4. Time dependence and smaller continents

To this point, we have dealt solely with supercontinents covering 30% of the surface. Fig. 5 shows continental and oceanic RMS velocities over 3000 Myr for cases identical to those in Fig. 4, except that the continents cover only 10% or 3% of the surface, similar to present-day Asia or Antarctica, respectively.

All panels of Fig. 5 reveal the same disparity in RMS surface velocity between oceanic and continental regions that we noted for the supercontinent cases. Continents move on average a factor of three slower than oceanic regions, except in the isoviscous, internally heated models, where they are again nearly stationary. However, the velocities of the smaller continents exhibit more temporal variation. The velocities of Asia-sized continents (top four panels) take on the comparatively broad range of 0–5 cm/yr, with the largest variations occurring in models with depth-dependent viscosity. For example, in the bottom-heated, layered viscosity case 2 continental velocities range between ~ 0–4 cm/yr on time scales of about 500 Myr. The internally heated, layered viscosity case 4 shows rapid velocity variations, between 2 and 5 cm/yr.

The bottom panels of Fig. 5 show that even smaller, Antarctica-sized continents exhibit the most rapid variations in continental velocity. For the bottom-heated, layered viscosity case 2 the continent spends as long as 500 Myr at velocities of ~ 1 cm/yr, interrupted by 400–500 Myr bursts in velocity of up to 4 cm/yr. The internally heated, layered viscosity case 4 shows the most dramatic variations in velocity, with bursts from 1 to 7 cm/yr over periods of ~ 100 Myr. This time scale is almost an order of magnitude shorter than that observed for velocity variations in the same case with a supercontinent (Fig. 4).

We summarize the temporal character of the motion of differently sized continents in Fig. 6. For simplicity we plot continental wander paths on Earth's surface for the final 1000 Myr of model integration

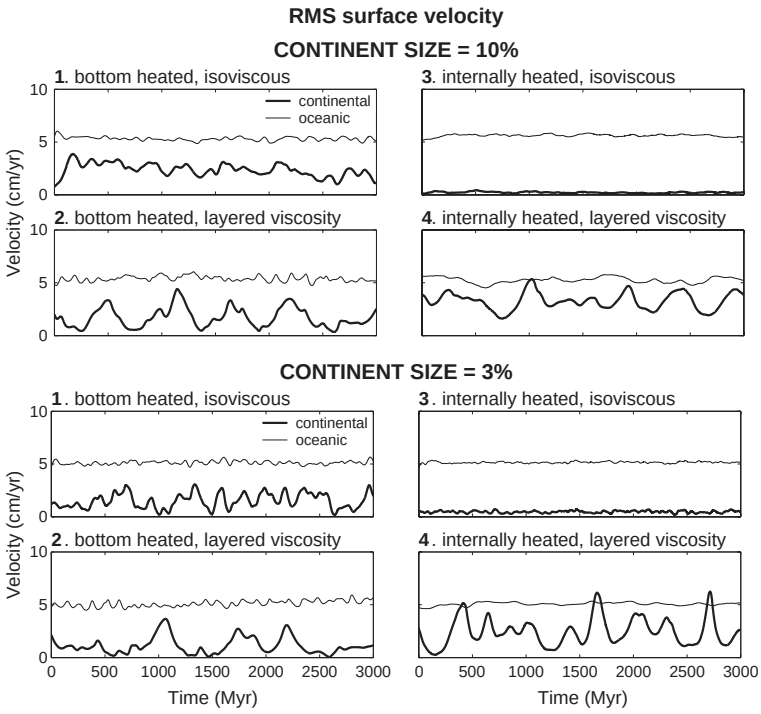

Fig. 5. RMS surface velocities for continents (thick lines) and the oceans (thin lines) for four cases identical to those shown in Fig. 4, save that the continents are smaller. Top: Continents cover 10% of the surface (approx. Asia). Continental velocities are generally slower than oceanic velocities. For case 1, continental motion varies between l and 4 cm/yr. In case 2 the velocity oscillates from ~ 0 to 4 cm/yr with a period of 500–600 Myr. In case 3 the continent is almost stagnant. Velocities in case 4 vary between 2 and 5 cm/yr. Bottom: Continents cover 3% of the surface (approx. Antarctica). For case 1, continental velocity varies between 0 and 3 cm/yr. In case 2 the velocity oscillates from ~ 0 to 4 cm/yr with extended periods of slow motion (≤ 1 cm/yr) for ~ 500 Myr. In case 3 the continent motion is < 1 cm/yr. Continental velocity in case 4 varies from 0 to 7 cm/yr on time scales of 100 Myr, exceeding the oceanic velocity for periods of < 100 Myr.

time for the internally heated, layered viscosity case 4 only. The paths of the continent centers are plotted with markers every 100 Myr, for all three continent sizes. For better comparison, we rotate all drift paths to a common reference point beginning at the North Pole. It is clear from Fig. 6 that as continent size decreases, time dependence increases, and continental trajectories become more erratic. For example, the

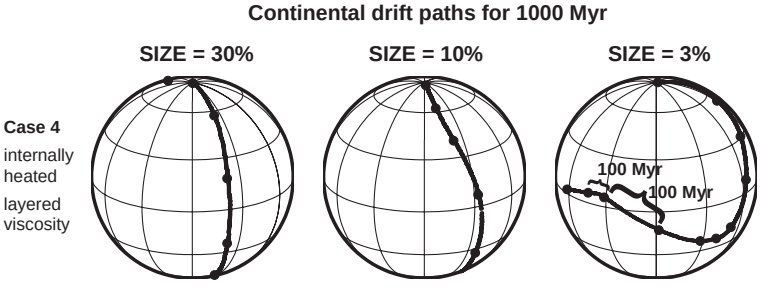

Fig. 6. Continental drift paths over the final 1000 Myr of evolution (from Figs. 4 and 5) for the internally heated, layered viscosity case 4. Paths are rotated to a reference frame beginning at the north pole. The path of the continent center is shown, with a marker every 100 Myr, for continents covering 30%, 10%, and 3% of the surface. Continental trajectory becomes more erratic and time dependence of motion increases as continent size decreases (note the disparate length of 100 Myr segments for the smallest continent).

supercontinent (left) follows a great circle path, and the arc length over any 100 Myr period varies by at most a factor of two, as expected from the RMS velocities in Fig. 4. The smaller continent covering 10% of the surface (middle) follows a more variable path, and the arc length traversed over any 100 Myr interval varies by a factor of three. The motion of the smallest continent, covering only 3% of the surface, exhibits the greatest time dependence. In this case we see changes in the course of the drift path by roughly 90° between 400 and 600 Myr, as well as periods of rapid velocity approaching 7 cm/yr followed by slow motion of less than 2 cm/yr, all within 100 Myr.

4. Discussion

We have investigated global mantle convection models with a freely moveable continent, focusing on the effects of bottom and internal heating, uniform and depth-dependent viscosity, and continental size. Still, we have by no means exhausted the relevant parameter space. In particular, our models do not include rigid oceanic plates. We expect large oceanic plates to impact convection. However, the addition of an oceanic lithosphere introduces significant difficulty into 3D spherical models. With a global lithosphere, plate geometries must evolve and plate boundary interactions must be treated explicitly. The addition of oceanic plates is of great interest for the future. However, we feel it essential to first understand the impact of continents before adding the complexity of an oceanic lithosphere. Another important shortcoming in our models is the lack of lateral viscosity variations due to temperature and stress heterogeneities in the mantle. We have also assumed that our model continents are perfectly rigid and cannot rift. Our choice of a reduced Rayleigh number relative to Earth's mantle is dictated primarily by computational considerations. In fact, each model calculation in our study takes about 2 weeks of integration time on a 128 processor Beowulf cluster, amounting to 6 months of computation. Therefore, we had to limit the range of parameters, highlighting key constraints on the convective planform.

Despite the apparent simplicity of these models there are important observations. For example, the dramatic effect of a supercontinent on the spectral heterogeneity character of the internally heated, layered viscosity model agrees well with earlier studies that show that Earth's long-wavelength convective planform is a straightforward result of combining strong plates at the surface with a high-viscosity lower mantle [31,32]. In other words, the peak in the geoid at spherical harmonic degree 2, with highs over Africa and the Pacific, arises primarily from prominent regions of subduction separated by buoyant continents, in a mantle with a strong radial increase in viscosity. The comparatively small effect of plumes in reddening the mantle heterogeneity spectrum moreover confirms earlier results by Lowman and Gable [9]. Using Cartesian mantle convection models, these authors showed that the effect of continental insulation is mainly a result of isolation from subduction, and that the focusing of plumes beneath a continent is in fact exaggerated in 2D mantle flow, owing to the inherent 3D nature of plumes.

Perhaps more surprising is the temporal behavior of our supercontinent models. In particular, the episodic motion of the supercontinent in our internally heated, layered viscosity model is striking, because it does not involve the effects of hot mantle plumes. Instead, feedback between the 15,000 km diameter supercontinent and the inherent ~ 10,000 km (spherical harmonic degree 4) length scales of flow lead to periods of relatively fast continental motion (4–5 cm/yr), punctuated by virtual stagnation (~ 1 cm/yr) over mantle downwellings. We note, however, that for the same case involving an isoviscous mantle, the continent remains nearly immobile. This contrast is due to the short wavelength planform of isoviscous mantle flow with internal heating, where numerous cold, downwelling plumes spaced by only ~ 2000 km exist at all times.

The time it takes for the supercontinent in the internally heated, layered viscosity case to advance after initially slowing down over a large downwelling is ~ 400 Myr. This is comparable to a mantle overturn time [57], and also agrees favorably with the rate suggested by the signature of the oldest slabs, which lag behind subduction zones long since shut off [58].

Our observation that the velocities of smaller continents are more episodic is consistent with previous 2D results [2]. Time dependence is greatest for the models with depth-dependent viscosity, where

the horizontal RMS velocities in the upper mantle are relatively large [30]. Peak velocities for Asia- and Antarctica-sized continents approach 7 cm/yr in the internally heated, layered viscosity mantle model. This is in agreement with paleomagnetic observations, which indicate that the velocities of some continents have been at times much higher than today [41]. Moreover, the time scale for these bursts in continental velocity is quite short, on the order of 100 Myr. Similar episodes are inferred from the paleomagnetic record for pre-Tertiary Gondwanaland, Eurasia, and North America [41], with the high velocity of India during the Cretaceous as the most recent example [46].

The primary intention of our models is the study of the dynamic feedback between global mantle flow and rigid continents. Consequently, we ignore the fact that oceanic areas also contain stiff plates. However, it is important to realize that the thermal boundary layer in the oceanic regions of our models is an integral part of the flow, as for the Earth. Moreover, the long wavelength flow associated with a layered viscosity mantle results in plate-like behavior even in the absence of a rigid oceanic lithosphere (e.g. [27]). We find that the RMS velocity of continents is on average smaller by a factor of three relative to oceanic regions, and similar ratios are in fact observed for plates on the Earth. For example, Forsyth and Uyeda [59] noted that at present predominantly oceanic plates move faster than continental plates by a factor of 3 to 4. Gordon and Jurdy [46] found analogous results for the Cenozoic. There has been speculation that the ocean/continent velocity difference results from deep keels associated with the continental tectosphere [60], but dynamic calculations show that this mechanism is largely ineffective [61,62]. Thus, the fact that this velocity difference arises naturally in our calculations is potentially of great interest.

5. Conclusions

We have systematically explored the effects of a moveable continent in several end-member global mantle convection models, isolating some key constraints on the nature of feedback between continents and the mantle. Supercontinents promote large-scale temperature anomalies primarily in models with depth-dependent viscosity and internal heating. Bottom heating also promotes long-wavelength heterogeneity through the clustering of plumes beneath the continent. Still, substantial short scale structure remains in isoviscous mantle flow even in the presence of a supercontinent. Supercontinents respond to long-wavelength mantle heterogeneity by following great circle paths, and their temporal velocity variations are amplified by an increase in lower mantle viscosity. Smaller continents exhibit bursts in velocity on time scales as short as 100 Myr. In all models we find an ocean/continent velocity difference, with continental velocities roughly a factor of three smaller than those in oceanic regions. This observation may help explain the inherent difference in the speed of predominantly oceanic or continental plates.

Acknowledgements

We thank Julian Lowman for thoughtful comments and Jason Morgan for many helpful discussions. This work was supported by NSF IGERT grant 1756252.

References

[1] D.L. Anderson, Hotspots, polar wander, Mesozoic convection and the geoid, Nature 297 (1982) 391–393.
[2] M. Gurnis, Large-scale mantle convection and the aggregation and dispersal of supercontinents, Nature 332 (1988) 695–699.
[3] L. Guillou, C. Jaupart, On the effect of continents on mantle convection, J. Geophys. Res. 100 (12) (1995) 24217–24238.
[4] A. Lenardic, W.M. Kaula, Mantle dynamics and the heat flow into the Earth's continents, Nature 378 (1995) 709–711.
[5] A. Lenardic, On the heat flow variation from Archean cratons to Proterozoic mobile belts, J. Geophys. Res. 102 (1) (1997) 709–721.
[6] S. Zhong, M. Gurnis, Dynamic feedback between a continent-like raft and thermal convection, J. Geophys. Res. 98 (7) (1993) 12219–12232.
[7] J.P. Lowman, G.T. Jarvis, Continental collisions in wide aspect ratio and high Rayleigh number two-dimensional mantle convection models, J. Geophys. Res. 101 (11) (1996) 25485–25497.
[8] J.P. Lowman, G.T. Jarvis, Effects of mantle heat source distribution on continental stability, J. Geophys. Res. 104 (6) (1999) 12733–12746.
[9] J.P. Lowman, C.W. Gable, Thermal evolution of the mantle following continental aggregation in 3D convection models, Geophys. Res. Lett. 26 (17) (1999) 2649–2652.

[10] M. Yoshida, Y. Iwase, S. Honda, Generation of plumes under a localized high viscosity lid in 3-D spherical shell convection, Geophys. Res. Lett. 26 (7) (1999) 947–950.
[11] G.J. Wasserburg, G.J.F. MacDonald, F. Hoyle, W.A. Fowler, Relative contributions of uranium, thorium, and potassium to heat production in the Earth, Science 143 (1964) 465–467.
[12] G.F. Davies, Ocean bathymetry and mantle convection: 1. Large-scale flow and hotspots, J. Geophys. Res. 93 (9) (1988) 10467–10480.
[13] N.H. Sleep, Hotspots and mantle plumes: some phenomenology, J. Geophys. Res. 95 (5) (1990) 6715–6736.
[14] L.H. Kellogg, B.H. Hager, R.D. van der Hilst, Compositional stratification in the deep mantle, Science 283 (1999) 1881–1884.
[15] G.A. Glatzmaier, P.H. Roberts, A three-dimensional self-consistent computer simulation of a geomagnetic field reversal, Nature 377 (1995) 203–209.
[16] W. Kuang, J. Bloxham, A numerical dynamo model in an Earth-like dynamical regime, Nature 389 (1997) 371–374.
[17] B. Buffett, Estimates of heat flow in the deep mantle based on the power requirements for the geodynamo, Geophys. Res. Lett. 29 (12) (2002) 1566, doi:10.1029/2001GL014649.
[18] R. Jeanloz, S. Morris, Is the geotherm sub-adiabatic in the lower mantle?, Geophys. Res. Lett. 14 (4) (1987) 335–338.
[19] H.-P. Bunge, Y. Ricard, J. Matas, Non-adiabaticity in mantle convection, Geophys. Res. Lett. 28 (5) (2001) 879–882.
[20] W.J. Su, A.M. Dziewonski, Predominance of long-wavelength heterogeneity in the mantle, Nature 352 (1991) 121–126.
[21] S.P. Grand, R.D. van der Hilst, S. Widiyantoro, Global seismic tomography: a snapshot of convection in the Earth, GSA Today 7 (4) (1997) 1–7.
[22] R.D. van der Hilst, S. Widiyantoro, E.R. Engdahl, Evidence for deep mantle circulation from global tomography, Nature 386 (1997) 578–584.
[23] J. Ritsema, H.J. van Heijst, J.H. Woodhouse, Complex shear wave velocity structure imaged beneath Africa and Iceland, Science 286 (1999) 1925–1928.
[24] M.A. Richards, D.C. Engebretson, Large-scale mantle convection and the history of subduction, Nature 355 (1992) 437–440.
[25] C. Litbgow-Bertelloni, M.A. Richards, The dynamics of Cenozoic and Mesozoic plate motions, Rev. Geophys. 36 (1) (1998) 27–28.
[26] M.A. Richards, B.H. Hager, N.H. Sleep, Dynamically supported geoid highs over hotspots; observation and theory, J. Geophys. Res. 93 (7) (1988) 7690–7708.
[27] H.-P. Bunge, M.A. Richards, J.R. Baumgardner, Effect of depth-dependent viscosity on the planform of mantle convection, Nature 379 (1996) 436–438.
[28] P.J. Tackley, On the ability of phase transitions and viscosity layering to induce long-wavelength heterogeneity in the mantle, Geophys. Res. Lett. 23 (15) (1996) 1985–1988.
[29] D.G. Bercovici, G.A. Schubert, G.A. Glatzmaier, Influence of heating mode on three-dimensional mantle convection, Geophys. Res. Lett. 16 (7) (1989) 617–620.
[30] H.-P. Bunge, M.A. Richards, J.R. Baumgardner, A sensitivity study of 3-D spherical mantle convection at 10^8 Rayleigh number: effects of depth-dependent viscosity, heating mode and an endothermic phase change, J. Geophys. Res. 102 (6) (1997) 11991–12007.
[31] H.-P. Bunge, M.A. Richards, The origin of large scale structure in mantle convection: effects of plate motions and viscosity structure, Geophys. Res. Lett. 23 (21) (1996) 2987–2990.
[32] M.A. Richards, W.-S. Yang, J.R. Baumgardner, H.-P. Bunge, Role of a low-viscosity zone in stabilizing plate tectonics: implications for comparative terrestrial planetology, Geochem. Geophys. Geosyst. 2 (2001) , doi:10.1029/2000GC000115.
[33] B.H. Hager, M.A. Richards, Long-wavelength variations in Earth's geoid: physical models and dynamical implications, Philos. Trans. R. Soc. Lond. 328 (1989) 309–327.
[34] S.D. King, G. Masters, An inversion for radial mantle viscosity structure using seismic tomography, Geophys. Res. Lett. 19 (15) (1992) 1551–1554.
[35] J.X. Mitrovica, Haskell [1935] revisited, J. Geophys. Res. 101 (1) (1996) 555–569.
[36] R. Trompert, U. Hansen, Mantle convection simulations with rheologies that generate plate-like behavior, Nature 395 (1998) 686–689.
[37] P.J. Tackley, Self-consistent generation of tectonic plates in time-dependent, pseudoplastic yielding, Geochem. Geophys. Geosyst. 1 (2000) , doi:10.1029/2000GC000036.
[38] P.J. Tackley, Self-consistent generation of tectonic plates in time-dependent, three-dimensional mantle convection simulations: 2. Strain weakening and asthenosphere, Geochem. Geophys. Geosyst. 1 (2000) , doi:10.1029/2000GC000043.
[39] R.V. der Voo, Paleomagnetism of the Atlantic, Tethys, and Iapetus Oceans, Cambridge University Press, Cambridge, UK, 1993.
[40] J.G. Meert, R.V. der Voo, C.M. Powell, Z.-X. Li, M.W. McElhinny, Z. Chen, D.T.A. Symons, A plate–tectonic speed limit?, Nature 363 (1993) 216–217.
[41] R.G. Gordon, M.O. McWilliams, A. Cox, Pre-Tertiary velocities of the continents: a lower bound from paleomagnetic data, J. Geophys. Res. 84 (10) (1979) 5480–5486.
[42] V. Courtillot, J. Besse, Magnetic field reversals, polar wander, and core–mantle coupling, Science 237 (1987) 1140–1147.
[43] J.L. Kirschvink, R.L. Ripperdan, D.A. Evans, Evidence for a large-scale Early Cambrian reorganization of continental masses by inertial interchange true polar wander, Science 277 (1997) 541–545.
[44] D.A.D. Evans, True polar wander and supercontinents, Tectonophysics 362 (2003) 303–320.
[45] J.B. Minster, T.H. Jordan, Present-day plate motions, J. Geophys. Res. 83 (11) (1978) 5331–5354.
[46] R.G. Gordon, D.M. Jurdy, Cenozoic global plate motions, J. Geophys. Res. 91 (12) (1986) 12389–12406.
[47] G.T. Jarvis, D.P. McKenzie, Convection in a compressible fluid with infinite Prandtl number, J. Fluid Mech. 96 (1980) 515–583.
[48] J.R. Baumgardner, Three dimensional treatment of convective flow in the Earth's mantle, J. Stat. Phys. 39 (5) (1985) 501–511.
[49] H.-P. Bunge, J.R. Baumgardner, Mantle convection modeling on parallel virtual machines, Comput. Phys. 9 (2) (1995) 207–215.

[50] G.F. Davies, Dynamic Earth, Cambridge University Press, Cambridge, UK, 1999.
[51] D.L. Turcotte, G. Schubert, Geodynamics, Cambridge University Press, Cambridge, UK, 2002.
[52] N.A. Haskell, The motion of a viscous fluid under a surface load, Physics 6 (1935) 265–269.
[53] G.F. Davies, Stirring geochemistry in mantle convection models with stiff plates and slabs, Geochim. Cosmochim. Acta 66 (2002) 3125–3142.
[54] J.G. Sclater, C. Jaupart, D. Galson, The heat flow through oceanic and continental crust and the heat loss of the Earth, Rev. Geophys. 18 (1) (1980) 269–311.
[55] C.W. Gable, R.J. O'Connell, B.J. Travis, Convection in three dimensions with surface plates: generation of toroidal flow, J. Geophys. Res. 96 (5) (1991) 8391–8405.
[56] P.J. Tackley, D.J. Stevenson, G.A. Glatzmaier, G. Schubert, Effects of multiple phase transitions in a three-dimensional spherical model of convection in Earth's mantle, J. Geophys. Res. 99 (8) (1994) 15877–15901.
[57] H.-P. Bunge, M.A. Richards, C. Lithgow-Bertelloni, J.R. Baumgardner, S.P. Grand, B. Romanowicz, Time scales and heterogeneous structure in geodynamic Earth models, Science 280 (1998) 91–95.
[58] G.F. Davies, Lagging mantle convection, the geoid and mantle structure, Earth Planet. Sci. Lett. 69 (1984) 187–194.
[59] D. Forsyth, S. Uyeda, On the relative importance of the driving forces of plate motion, Geophys. J. R. Astron. Soc. 43 (1975) 163–200.
[60] T.H. Jordan, The continental tectosphere, Rev. Geophys. 13 (3) (1975) 1–12.
[61] P.R. Stoddard, D. Abbott, Influence of the tectosphere upon plate motion, J. Geophys. Res. 101 (3) (1996) 5425–5433.
[62] S. Zhong, Role of ocean-continent contrast and continental keels on plate motion, net rotation of lithosphere, and the geoid, J. Geophys. Res. 106 (1) (2001) 703–712.